[Research Paper] 대한금속 · 재료학회지 (*Korean J. Met. Mater.*), Vol. 59, No. 5 (2021) pp.329-335
DOI: 10.3365/KJMM.2021.59.5.329

Charge Transport and Thermoelectric Properties of Mn-Doped Tetrahedrites $Cu_{12-x}Mn_xSb_4S_{13}$

Sung-Yoon Kim, Go-Eun Lee, and Il-Ho Kim*

Department of Materials Science and Engineering, Korea National University of Transportation, Chungju 27469, Republic of Korea

Abstract: Mn-doped tetrahedrites $Cu_{12-x}Mn_xSb_4S_{13}$ ($0.1 \le x \le 0.4$) were synthesized by mechanical alloying (MA) and sintered by hot pressing (HP). A single tetrahedrite phase was synthesized by MA without post-annealing, and it was stable without any phase changes after HP. The hot-pressed specimens had a relative density higher than 98.6%. The lattice constant of the Mn-doped samples increased compared to that of undoped $Cu_{12}Sb_4S_{13}$, but no significant change in the lattice constant was observed with a change in Mn content. All Mn-doped tetrahedrites acted as p-type semiconductors, as confirmed from positive Hall and Seebeck coefficient values. The Seebeck coefficient increased with increasing temperature but decreased with increasing Mn content; maximum Seebeck coefficient values of 200–219 μVK^{-1} were obtained at 323–723 K for $x = 0.1$. Electrical conductivity increased with increasing temperature and Mn content; the highest electrical conductivity values of $(1.76–2.45) \times 10^4$ Sm^{-1} were obtained at 323–723 K for $x = 0.4$. As a result, $Cu_{11.6}Mn_{0.4}Sb_4S_{13}$ exhibited a maximum power factor of 0.80 $mWm^{-1}K^{-2}$ at 723 K. As the Mn content increased, both the electronic and lattice thermal conductivities increased, and thus, the total thermal conductivity was the lowest at 0.48–0.63 $Wm^{-1}K^{-1}$ at 323–723 K for $x = 0.1$. A maximum dimensionless figure of merit of 0.75 was obtained at 723 K for $Cu_{11.7}Mn_{0.3}Sb_4S_{13}$. The MA-HP process is suitable for preparing doped tetrahedrites exhibiting excellent thermoelectric performance.

(Received February 18, 2021; Accepted March 2, 2021)

Keywords: thermoelectric, tetrahedrite, charge transport, mechanical alloying, hot pressing

1. Introduction

Tetrahedrite ($Cu_{12}Sb_4S_{13}$) is an earth-abundant sulfosalt mineral composed of low-cost and eco-friendly elements, and lacks toxic elements such as Pb or Te. In addition, it has the characteristics of a p-type thermoelectric material and exhibits a high dimensionless figure of merit (ZT) at temperatures near 723 K [1-4]. The tetrahedrite has 58 atoms arranged in a complex crystal structure in a highly symmetrical cubic unit cell (space group $I\bar{4}3m$) consisting of CuS_4 tetrahedra, CuS_3 triangles, and SbS_3 pyramids [5]. Within the tetrahedrite structure, Cu, Sb, and S exist as $Cu^{+}_{10}Cu^{2+}_{2}Sb^{3+}_{4}S^{2-}_{13}$ [6]. A Cu^+ ion located inside a triangular plane of three S atoms vibrates at high frequency with low energy because of the attractive and repulsive forces of the lone-pair electrons of Sb, thus inducing inherently low lattice thermal conductivity by interfering with heat transfer [7-9]. Studies have been conducted to improve the thermoelectric performance of tetrahedrite by partially substituting Cu^+, Sb^{3+}, or S^{2-} sites with other elements. When Cu^+ ions are substituted with transition atoms with an oxidation state of 2+ or 3+, additional electrons are generated, and the carrier concentration changes, resulting in changes in the charge transport and thermoelectric properties of tetrahedrite.

Pi *et al*. [10] investigated the thermal stability, mechanical properties, and thermoelectric properties of $Cu_{11}TrSb_4S_{13}$ (Tr = Mn/Fe/Co/Ni/Cu/Zn), and reported a ZT of 0.66 at 723 K for $Cu_{12}Sb_4S_{13}$. Tippireddy *et al*. [11] studied the projected density of states, magnetic properties, and thermoelectric properties of $Cu_{12-x}Tr_xSb_4S_{13}$ (x = 0.5 for Tr = Fe/Mn and x = 1 for Tr = Cu/Co/Ni/Zn) and obtained a ZT of 0.89 at 700 K for $Cu_{11.5}Mn_{0.5}Sb_4S_{13}$. In our previous studies, high ZT values were achieved for tetrahedrites by doping with transition atoms: ZT = 0.94 at 723 K for $Cu_{11.8}Co_{0.2}Sb_4S_{13}$ [12], ZT = 0.92 at 723 K for $Cu_{11.8}Ni_{0.2}Sb_4S_{13}$ [13], ZT = 0.80 at 723 K for $Cu_{11.8}Fe_{0.2}Sb_4S_{13}$ [14], and ZT = 0.76 at 723 K for $Cu_{11.6}Zn_{0.4}Sb_4S_{13}$ [15]. Chetty *et al*. [16] examined the elastic, magnetic, and thermoelectric properties of Cu_{12-}

- 김성윤: 석사과정, 이고은: 박사과정, 김일호: 교수
*Corresponding Author: Il-Ho Kim
[Tel: +82-43-841-5387, E-mail: ihkim@ut.ac.kr]

$_xMn_xSb_4S_{13}$ (x = 0–1.8). As a result, they achieved a ZT of 0.76 at 623 K for $Cu_{12}Sb_4S_{13}$, and among their Mn-doped samples, $Cu_{11.6}Mn_{0.4}Sb_4S_{13}$ exhibited the highest ZT of 0.64 at 673 K. Wang *et al*. [17] studied the thermoelectric properties of $Cu_{12-x}Mn_xSb_4S_{13}$ (x = 0–2) and obtained a ZT of 0.89 at 700 K for $Cu_{11.5}Mn_{0.5}Sb_4S_{13}$. Guélou *et al*. [18] analyzed the atomic displacement parameters to confirm the low-energy vibration of Cu atoms in $Cu_{12-x}Mn_xSb_4S_{13}$ (x = 0 and 1) and achieved a ZT of 0.56 at 573 K for $Cu_{11}MnSb_4S_{13}$.

Because the boiling temperature of S is lower than the melting temperature of Cu, the synthesis of tetrahedrite using a typical melting method requires a sophisticated heating-maintenance-cooling process and long-duration annealing (usually one to two weeks) to achieve phase transformation and homogenization [19,20]. However, mechanical alloying (MA) is a low-temperature process, and as a result, volatilization and segregation of component elements do not occur, which is advantageous for the homogenization of the synthetic phase [21]. In our previous study [22], we determined the optimal process conditions for synthesizing $Cu_{12}Sb_4S_{13}$ with MA and hot pressing (HP), and a single tetrahedrite phase was obtained within 24 h without post-annealing. In this study, Mn-doped tetrahedrites were prepared using the MA-HP method, and their charge-transport parameters and thermoelectric properties were examined.

2. Experimental Procedure

Mn-doped tetrahedrites $Cu_{12-x}Mn_xSb_4S_{13}$ (x = 0.1, 0.2, 0.3, and 0.4) were synthesized by MA. Elemental powders of Cu (<45 μm, purity 99.9%, Kojundo), Mn (<45 μm, purity 99.9%, LTS), Sb (<150 μm, purity 99.999%, Kojundo), and S (<75 μm, purity 99.99%, Kojundo) were mixed in a stoichiometric ratio. Next, 20 g of the mixed powder and 400 g of 5 mm-diameter stainless steel balls were placed in a hardened steel jar. After the inside of the jar was evacuated, Ar gas was injected and MA was performed for 24 h at a rotation speed of 350 rpm using a planetary ball mill (Fritsch Pulverisette5). The synthesized powder was loaded onto a graphite mold, and HP was conducted at 723 K for 2 h under 70 MPa in vacuum. Details of the MA-HP process have been reported in our previous study [22].

The phases of the hot-pressed specimens were analyzed using X-ray diffraction (XRD; Bruker D8-Advance) with Cu Kα radiation (θ-2θ mode; step size: 0.02 °; scan speed: 0.4 s/step). The lattice constant was calculated using the Rietveld refinement (TOPAS software). Scanning electron microscopy (SEM; FEI Quanta400) and energy-dispersive X-ray spectroscopy (EDS; Bruker Quantax200) were employed to observe the microstructures of the HP specimens. Through elemental mapping, the homogeneous distribution of the elements was confirmed. Charge transport parameters (Hall coefficient, mobility, and carrier concentration) were examined using the van der Pauw method (Keithley 7065) by applying a direct current of 100 mA and a constant magnetic field of 1 T. The electrical conductivity (σ) and Seebeck coefficient (α) were measured simultaneously in the temperature (T) range from 323 to 723 K using a Ulvac-Riko ZEM-3 system in He atmosphere. Thermal conductivity (κ) was determined using the density, specific heat, and thermal diffusivity as measured by the Ulvac-Riko TC-9000H equipment. Finally, the power factor ($PF = \alpha^2\sigma$) and dimensionless figure of merit ($ZT = \alpha^2\sigma\kappa^{-1}T$) were evaluated.

3. Results and Discussion

Fig. 1 presents the XRD patterns of Mn-doped tetrahedrite $Cu_{12-x}Mn_xSb_4S_{13}$ specimens synthesized by the MA-HP process. All specimens contained only a single tetrahedrite phase without secondary phases. No significant change was observed in the lattice constant (1.0374–1.0379 nm) with a

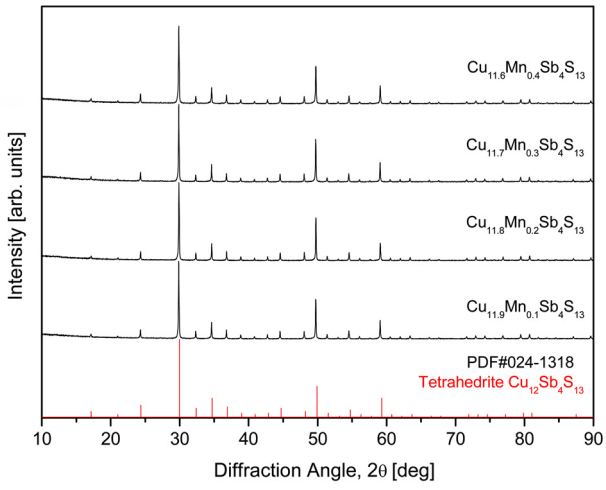

Fig. 1. XRD patterns of $Cu_{12-x}Mn_xSb_4S_{13}$ tetrahedrites prepared by the MA-HP process.

Table 1. Chemical compositions and physical properties of $Cu_{12-x}Mn_xSb_4S_{13}$.

Composition		Relative density [%]	Lattice constant [nm]	Lorenz number [10^{-8} V^2K^{-2}]
Nominal	Actual			
$Cu_{11.9}Mn_{0.1}Sb_4S_{13}$	$Cu_{11.80}Mn_{0.15}Sb_{4.27}S_{12.77}$	99.8	1.0375	1.68
$Cu_{11.8}Mn_{0.2}Sb_4S_{13}$	$Cu_{12.26}Mn_{0.19}Sb_{4.15}S_{12.40}$	99.2	1.0374	1.73
$Cu_{11.7}Mn_{0.3}Sb_4S_{13}$	$Cu_{11.36}Mn_{0.32}Sb_{4.28}S_{13.04}$	98.8	1.0379	1.76
$Cu_{11.6}Mn_{0.4}Sb_4S_{13}$	$Cu_{11.46}Mn_{0.46}Sb_{4.13}S_{12.95}$	98.6	1.0374	1.82

change in Mn content, as shown in Table 1. However, the lattice constant of doped samples increased compared to that of undoped $Cu_{12}Sb_4S_{13}$ (1.0350 nm) [10]. This confirmed the successful substitution (doping) of Mn for the Cu sites, because the ionic radius of Mn^{2+} (66 pm) is larger than that of Cu^+ (60 pm). Chetty *et al*. [16] reported an increased lattice constant of 1.043 nm for $Cu_{10.2}Mn_{1.8}Sb_4S_{13}$ compared to 1.032 nm for $Cu_{12}Sb_4S_{13}$. Guélou *et al*. [18] also obtained similar results of 1.0323 nm for $Cu_{12}Sb_4S_{13}$ and 1.0386 nm for $Cu_{11}MnSb_4S_{13}$, showing a significantly increased lattice constant due to Mn substitution. In this study, the amount of Mn substitution (x = 0.1–0.4) was less than that used in other studies, and thus, the increase in lattice constant was not large.

Fig. 2 displays SEM images of hot-pressed Cu_{12-x} Mn_x Sb_4S_{13}. No significant difference in microstructure with a change in Mn content was observed, indicating a densely sintered microstructure with few pores. As shown in Table 1, all specimens exhibited high relative densities of 98.6%–99.8%, and there was no remarkable difference between the nominal and actual compositions. In particular, the composition change resulting from the volatilization of S, which is easily generated in the melting process, was suppressed. The EDS elemental maps showed that each element of $Cu_{11.7}Mn_{0.3}$ Sb_4S_{13} was homogeneously distributed. In this study, the volatilization of the component elements was suppressed, and compact sintering was successfully achieved using the solid-state MA-HP process.

Fig. 3 shows the carrier concentration and mobility of $Cu_{12-x}Mn_xSb_4S_{13}$. The change in the carrier (hole) concentration according to the Mn content was not large. However, the mobility increased with increasing Mn content. When Cu was substituted by Mn, the additionally generated electrons did not meet the expectation that the carrier concentration would decrease due to a reduction in hole concentration (charge compensation). All specimens exhibited positive Hall coefficients, indicating p-type conduction. However, the Hall coefficient values measured in this study were unreliable because a different value was obtained for each measurement. Many studies have failed to effectively measure the Hall coefficient of tetrahedrite [3,11].

The thermoelectric properties of $Cu_{12-x}Mn_xSb_4S_{13}$ were

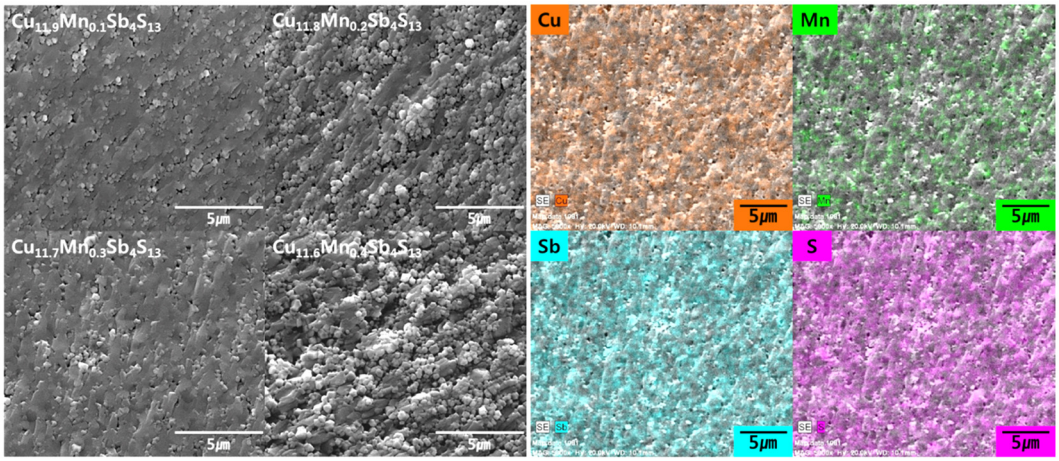

Fig. 2. SEM images of hot-pressed $Cu_{12-x}Mn_xSb_4S_{13}$ and EDS elemental maps of $Cu_{11.7}Mn_{0.3}Sb_4S_{13}$.

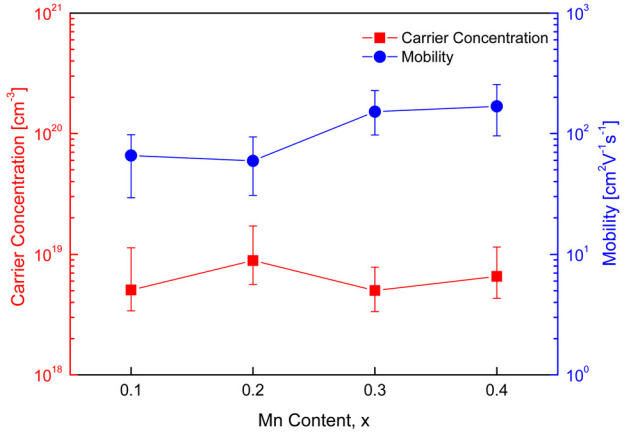

Fig. 3. Charge transport properties of $Cu_{12-x}Mn_xSb_4S_{13}$.

measured and examined in the temperature range of 323–723 K. Fig. 4 presents the Seebeck coefficient of $Cu_{12-x}Mn_xSb_4S_{13}$. Positive Seebeck coefficient values were found for all specimens, suggesting that the major carriers were holes of p-type semiconductors. The Seebeck coefficient is expressed as the relation: $\alpha = (8/3)\pi^2 k_B^2 m^* T e^{-1} h^{-2} (\pi/3n)^{2/3}$, where k_B is the Boltzmann constant, m^* is the effective carrier mass, e is the electronic charge, h is the Planck constant, and n is the carrier concentration [23]. The Seebeck coefficient increases as the temperature increases, but when the temperature exceeds a certain temperature (intrinsic transition temperature), the carrier concentration increases rapidly and thus the Seebeck coefficient decreases. As a result, the Seebeck coefficient of a p-type semiconductor decreases after showing a peak value at a specific temperature. In this study, as the temperature

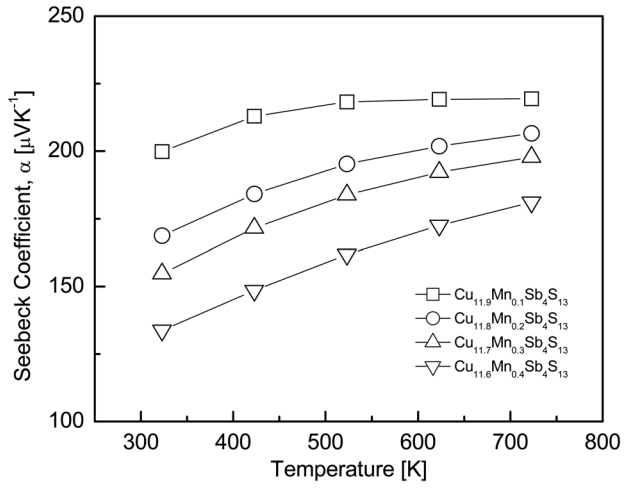

Fig. 4. Seebeck coefficient of $Cu_{12-x}Mn_xSb_4S_{13}$.

increased, the Seebeck coefficient increased for all specimens. This implied that no intrinsic transition occurred in the measured temperature range of 323–723 K.

As the Mn content increased at a constant temperature, the Seebeck coefficient decreased and its temperature dependence greatly increased. $Cu_{11.9}Mn_{0.1}Sb_4S_{13}$ exhibited the highest Seebeck coefficient value of 200–219 μVK^{-1} at 323–723 K. This was higher than the 155–195 μVK^{-1} at 323–723 K for undoped $Cu_{12}Sb_4S_{13}$ obtained by Pi *et al*. [10]. Therefore, the partial substitution of Mn at the Cu sites led to an increase in the Seebeck coefficient of tetrahedrite. However, it decreased to 134–181 μVK^{-1} at the same temperature for $Cu_{11.6}Mn_{0.4}Sb_4S_{13}$. Chetty *et al*. [16] reported increased Seebeck coefficient values from 90–142 μVK^{-1} for $Cu_{12}Sb_4S_{13}$ to 96–150 μVK^{-1} for $Cu_{11.6}Mn_{0.4}Sb_4S_{13}$, and 287–400 μVK^{-1} for $Cu_{10.2}Mn_{1.8}Sb_4S_{13}$ at 300–723 K with increasing Mn substitution. Wang *et al*. [17] obtained approximately three-times higher values of 250–325 μVK^{-1} for $Cu_{10}Mn_2Sb_4S_{13}$ compared to 77–134 μVK^{-1} for undoped $Cu_{12}Sb_4S_{13}$ at temperatures from 300 to 700 K, and they interpreted the reason for the increased Seebeck coefficient: the carrier (hole) concentration decreased because the divalent or trivalent transition element was substituted at the Cu^+ sites. In this study, although the Seebeck coefficient was increased by Mn doping compared to that of the undoped tetrahedrite, the reason why the Seebeck coefficient decreased with increasing Mn content is still questionable.

Fig. 5 shows the temperature dependence of the electrical conductivity of $Cu_{12-x}Mn_xSb_4S_{13}$. The electrical conductivity increased as the temperature increased and decreased slightly at temperatures above 723 K for only $Cu_{11.6}Mn_{0.4}Sb_4S_{13}$. This means that the Mn-doped tetrahedrites behave as nondegenerate semiconductors. The electrical conductivity at a constant temperature increased with increasing Mn content. In this study, the highest electrical conductivity values of (1.8–2.4) $\times 10^4$ Sm^{-1} were obtained for $Cu_{11.6}Mn_{0.4}Sb_4S_{13}$ in the temperature range of 323–723 K. These values were slightly higher than those for undoped $Cu_{12}Sb_4S_{13}$, (1.1–1.9) $\times 10^4$ Sm^{-1} at 323–723 K[10]. Mn doping resulted in the opposite trend of what was expected, a decrease in electrical conductivity owing to the decreased hole concentration. Chetty *et al*. [16] obtained electrical resistivities of 1.013 and 1.693 mΩcm at 300 K for $Cu_{12}Sb_4S_{13}$ and $Cu_{11.6}Mn_{0.4}Sb_4S_{13}$,

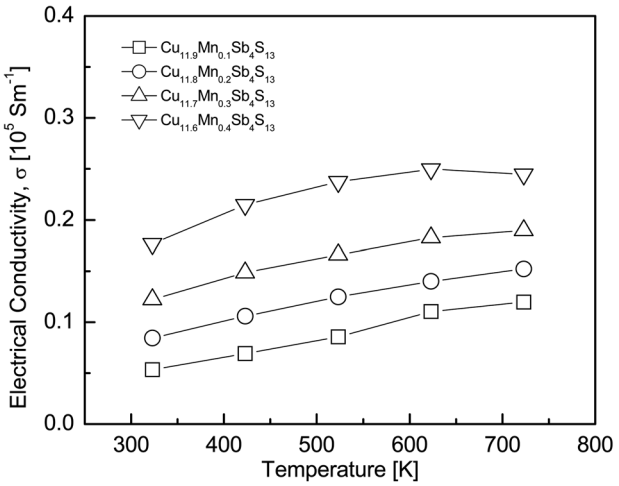

Fig. 5. Electrical conductivity of $Cu_{12-x}Mn_xSb_4S_{13}$.

respectively, with little dependence on temperature, and reported that the electrical resistivity increased (the electrical conductivity increased) to 181–66 mΩcm at 300–723 K for $Cu_{10.2}Mn_{1.8}Sb_4S_{13}$. Wang *et al*. [17] obtained an electrical conductivity of $(8.6–6.5) \times 10^4$ Sm^{-1} at 300–700 K for $Cu_{12}Sb_4S_{13}$, a decrease with increasing temperature, and reported an electrical conductivity of 0.1×10^4 Sm^{-1} at 300 K for $Cu_{10}Mn_2Sb_4S_{13}$, a decrease with increasing Mn content with little temperature dependence.

Fig. 6 presents the power factor (PF) of $Cu_{12-x}Mn_xSb_4S_{13}$. Because carrier concentration affects both the Seebeck coefficient and the electrical conductivity, optimization of the carrier concentration is necessary to obtain a high PF value.

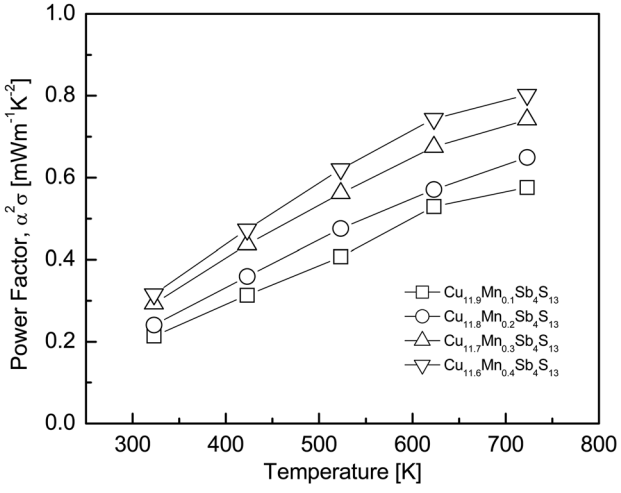

Fig. 6. Power factor of $Cu_{12-x}Mn_xSb_4S_{13}$.

In this study, the PF increased with increasing temperature within the measured temperature range because it did not exceed the intrinsic transition temperature. As the Mn content increased, the PF increased because the increase in electrical conductivity was dominant over the reduction in Seebeck coefficient by Mn doping. In the case of $Cu_{11.6}Mn_{0.4}Sb_4S_{13}$, despite having the lowest Seebeck coefficient, the highest PF values of 0.32–0.80 $mWm^{-1}K^{-2}$ were obtained in the temperature range of 323–723 K owing to its highest electrical conductivity. However, Mn doping was not effective at increasing the PF of tetrahedrite; Chetty *et al*. [16] obtained a maximum PF of 1.7 $mWm^{-1}K^{-2}$ at 623 K for $Cu_{12}Sb_4S_{13}$, which decreased to 1.2 $mWm^{-1}K^{-2}$ at 623 K for $Cu_{11.6}Mn_{0.4}Sb_4S_{13}$. Wang *et al*. [17] reported a maximum PF of 1.2 $mWm^{-1}K^{-2}$ at 700 K for $Cu_{12}Sb_4S_{13}$, which decreased to

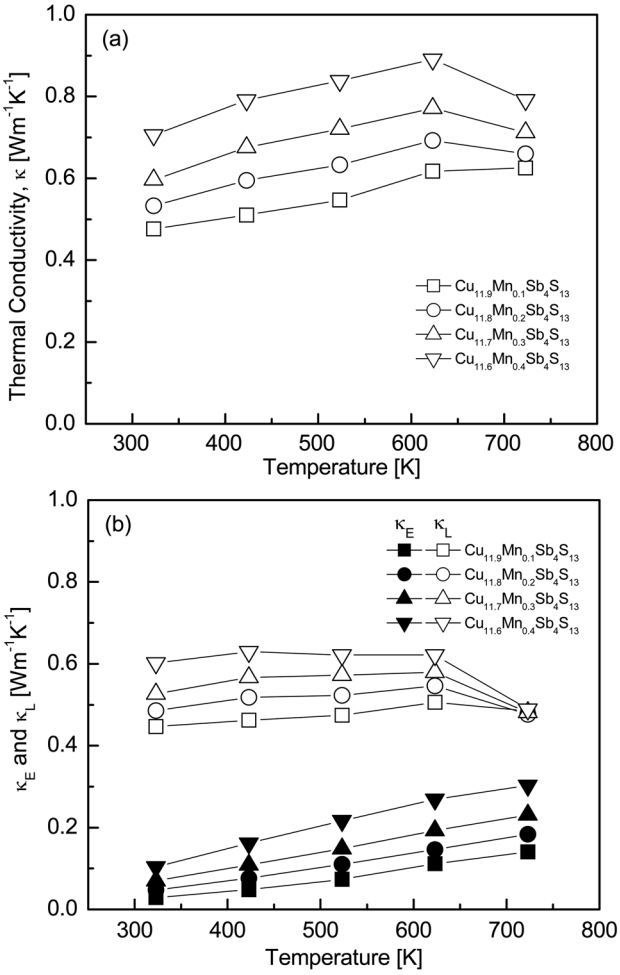

Fig. 7. Thermal conductivity of $Cu_{12-x}Mn_xSb_4S_{13}$: (a) total thermal conductivity and (b) electronic and lattice thermal conductivities.

0.9 $mWm^{-1}K^{-2}$ at 675 K for $Cu_{11.5}Mn_{0.5}Sb_4S_{13}$.

Fig. 7 shows the temperature dependence of thermal conductivity of $Cu_{12-x}Mn_xSb_4S_{13}$. The maximum total thermal conductivity of all specimens was observed at 623 K, and it increased with increasing Mn content at a constant temperature. The lattice thermal conductivity (κ_L) was calculated using the equation: $\kappa_L = \kappa - \kappa_E$, where κ is the total thermal conductivity and κ_E is the electronic thermal conductivity. The κ_E was estimated using the Wiedemann–Franz law ($\kappa_E = L\sigma T$, L: Lorenz number) [24], where the Lorenz number [10^{-8} V^2K^{-2}] was obtained using the formula [25]. As shown in Table 1, as the Mn content increased, the Lorenz number increased from 1.68×10^{-8} to 1.82×10^{-8} V^2K^{-2} at 323 K. The electronic thermal conductivity increased with increasing temperature, but the total thermal conductivity increased with increasing temperature, reached a maximum at 623 K, and then decreased. This was due to the combined result of increasing electronic thermal conductivity with increasing temperature and decreasing lattice thermal conductivity at temperatures higher than 623 K. The electronic thermal conductivity was directly related to the electrical conductivity (carrier concentration) and Lorenz number, and thus, it increased with increasing Mn content. $Cu_{11.9}Mn_{0.1}Sb_4S_{13}$ exhibited the lowest lattice thermal conductivity, resulting in the lowest total thermal conductivity of 0.48–0.63 $Wm^{-1}K^{-1}$ at 323–723 K, where κ_E = 0.03–0.14 $Wm^{-1}K^{-1}$ and κ_L = 0.45–0.49 $Wm^{-1}K^{-1}$.

The dimensionless figure of merit (ZT) of $Cu_{12-x}Mn_xSb_4S_{13}$ is presented in Fig. 8. As the temperature increased, the ZT value increased because of the increase in the PF and the maintenance of low thermal conductivity. In our previous study [10], undoped $Cu_{12}Sb_4S_{13}$ exhibited a ZT of 0.66 at 723 K. In this study, as the Mn content increased, both the thermal conductivity and PF increased. As a result, $Cu_{11.7}Mn_{0.3}Sb_4S_{13}$ exhibited the highest ZT of 0.75 at 723 K. Wang *et al.* [17] reported a ZT of 0.89 at 700 K for $Cu_{11.5}Mn_{0.5}Sb_4S_{13}$ prepared by encapsulated melting and HP. Guélou *et al.* [18] obtained a ZT of 0.56 at 573 K for $Cu_{11}MnSb_4S_{13}$ produced by MA and HP. Wang *et al.* [17] performed long-term and careful melting processes; raw elements were heated to 923 K, maintained for 12 h, cooled to room temperature, and then annealed at 723 K for two weeks. Guélou *et al.* [18] also conducted long-term and multi-step processes; samples were mechanically alloyed for 6 h, annealed at 973 K for 3 h, and cooled to 823 K for 30 h. The furnace was then cooled to room temperature, and finally, the ingot was crushed and subjected to a second annealing at 823 K for 30 h. In the present study, however, a single tetrahedrite phase exhibiting a high level of ZT was obtained by MA within 24 h without post-annealing. Therefore, the MA-HP process is suitable for preparing doped tetrahedrites with excellent thermoelectric performance.

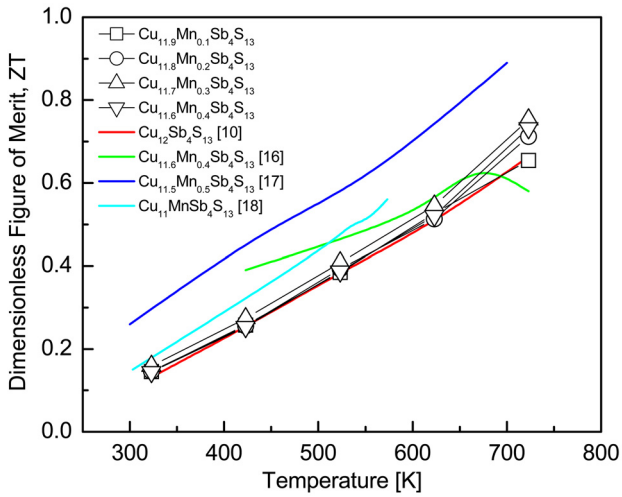

Fig. 8. Dimensionless figure of merit for $Cu_{12-x}Mn_xSb_4S_{13}$.

4. Conclusions

Mn-doped tetrahedrites $Cu_{12-x}Mn_xSb_4S_{13}$ (x = 0.1–0.4) were synthesized by MA, followed by HP. The hot-pressed specimens had a relative density higher than 98.6%. Positive Hall and Seebeck coefficient values were obtained, meaning that all of the Mn-doped tetrahedrites acted as p-type semiconductors. As the temperature increased, the Seebeck coefficient and electrical conductivity increased. As the Mn content increased, the Seebeck coefficient decreased but the electrical conductivity increased. The trend in electronic thermal conductivity was the same as that of electrical conductivity, and the minimum thermal conductivity was achieved for $Cu_{11.9}Mn_{0.1}Sb_4S_{13}$. The PF increased because of the increase in electrical conductivity with increasing Mn doping level. As a result, the maximum ZT value of 0.75 was obtained at 723 K for $Cu_{11.7}Mn_{0.3}Sb_4S_{13}$.

Acknowledgment

This study was supported by the Basic Science Research Capacity Enhancement Project (National Research Facilities and Equipment Center) through the Korea Basic Science Institute funded by the Ministry of Education (Grant No. 2019R1A6C1010047).

REFERENCES

1. X. Lu and D. T. Morelli, *Phys. Chem. Chem. Phys.* **15**, 5762 (2013).
2. K. Suekuni, K. Tsuruta, T. Ariga, and M. Koyano, *Appl. Phys. Exp.* **5**, 1201 (2012).
3. X. Lu, D. T. Morelli, Y. Xia, F. Zhou, V. Ozolins, H. Chi, X. Zhou, and C. Uher, *Adv. Energy Mater.* **3**, 342 (2013).
4. T. Barbier, P. Lemoine, S. Gascoin, O. I. Lebedev, A. Kaltzoglou, P. Vaqueiro, A. V. Powell, R. I. Smith, and E. Guilmeau, *J. Alloys Compd.* **634**, 253 (2015).
5. A. Pfitzner, M. Evain, and V. Petricek, *Acta Crystallogr.* **53**, 337 (1997).
6. R. Chetty, A. Bali, and R. C. Mallik, *J. Mater. Chem. C* **3**, 12364 (2015).
7. B. Lenoir, Y. Bouyrie, C. Candolfi, S. Pailhès, M. M. Koza, B. Malaman, A. Dauscher, J. Tobola, O. Boisron, and L. Saviot, *Chem. Phys.* **17**, 19751 (2015).
8. X. Lu, W. Lai, Y. Wang, and D. T. Morelli, *Adv. Funct. Mater.* **25**, 3648 (2015).
9. D. T. Morelli, E. Lara-Curzio, A. F. May, O. Delaire, M. A. McGuire, X. Lu, C. Y. Liu, and E. D. Case, *J. Appl. Phys.* **115**, 193515 (2014).
10. J. H. Pi, G. E. Lee, and I. H. Kim, *J. Electron. Mater.* **49**, 2710 (2020).
11. S. Tippireddy, R. Chetty, M. H. Naik, M. Jain, K. Chattopadhyay, and R. C. Mallik, *J. Phys. Chem.* **122**, 8735 (2018).
12. S. Y. Kim, G. E. Lee, and I. H. Kim, *J. Korean Phys. Soc.* **74**, 967 (2019).
13. S. Y. Kim, G. E. Lee, and I. H. Kim, *J. Electron. Mater.* **49**, 2775 (2020).
14. S.-Y. Kim, J.-H. Pi, G.-E. Lee, and I.-H. Kim, *Korean J. Met. Mater.* **58**, 340 (2020).
15. S.-G. Kwak, G.-E. Lee, and I.-H. Kim, *Korean J. Met. Mater.* **57**, 328 (2019).
16. R. Chetty, D. S. P. Kumar, G. Rogl, P. Rogl, E. Bauer, H. Michor, S. Suwas, S. Puchegger, G. Giester, and R. C. Mallik, *Phys. Chem. Chem. Phys.* **17**, 1716 (2015).
17. J. Wang, X. Li, and Y. Bao, *Mater. Sci. For.* **847**, 161 (2016).
18. G. P. L. Guélou, A. V. Powell, R. I. Smith, and P. Vaqueiro, *J. Appl. Phys.* **126**, 045107 (2019).
19. L. L. Huang, J. Zhang, Z. M. Wang, X. G. Zhu, J. M. Li, C. Zhu, D. Li, C. J. Song, H. X. Xin, and X. Y. Qin, *Materialia* **3**, 169 (2018).
20. A. F. May, O. Delaire, J. L. Niedziela, E. Lara-Curzio, M. A. Susner, D. L. Abernathy, M. Kirkham, and M. A. McGuire, *Phys. Rev. B* **93**, 064104 (2016).
21. Y. Q. Yu, B. P. Zhang, Z. H. Ge, P. P. Shang, and Y. X. Chen, *Mater. Chem. Phys.* **131**, 1 (2011).
22. S. Y. Kim, S. G. Kwak, J. H. Pi, G. E. Lee, and I. H. Kim, *J. Electron. Mater.* **48**, 1857 (2019).
23. G. J. Snyder and E. S. Toberer, *Nat. Mater.* **7**, 105 (2008).
24. H. Cailat, A. Borshchevsky, and J. P. Fleurial, *J. Appl. Phys.* **80**, 4442 (1996).
25. B. Madaval and S. J. Hong, *J. Electron. Mater.* **45**, 12 (2016).